Cyclic preservation of Fe/Mn-redox fronts in sediments of an oligotrophic, ventilated deep-water lake (Lago Fagnano, Tierra del Fuego)

Ina Neugebauer[1,*,#], Camille Thomas[1], Nicolas D. Waldmann[2], Cristina Recasens[1], and Daniel Ariztegui[1]

1 Department of Earth Sciences, University of Geneva, Rue des Maraichers 13, 1205 Geneva, Switzerland

2 Dr Moses Strauss Department of Marine Geosciences, Charney School of Marine Sciences, University of Haifa, Mount Carmel, 31905 Haifa, Israel

* Corresponding author; E-mail address: inaneu@gfz-potsdam.de

Present address: GFZ German Research Centre for Geosciences, Section 5.2 – Climate Dynamics and Landscape Evolution, Telegrafenberg, 14473 Potsdam, Germany

ABSTRACT

Changing redox conditions in lakes are captured in their sediments, and are often influenced by climate. Their study therefore allows tracing past climate change on (sub-) annual to longer time-scales. In Lago Fagnano (54°S Argentina/Chile), an oligotrophic and deep-ventilated soft-water lake, cyclic alternations of light grey clay and dark green to black laminae are preserved throughout the Holocene sedimentary record. This study aims at clarifying the mechanism, frequency, and climatic forcing of laminae formation and preservation in Lago Fagnano, and their relation to changing redox conditions in the lake. Using high-resolution XRF scanning and mapping, thin section, XRD and SEM analyses of sediment cores, Fe- and Mn-oxides were identified as generating the lamination on (sub-) decadal time-scales. Black and greenish laminae are interpreted as buried palaeo-oxidation fronts that underwent early diagenetic processes. The burial of redox fronts in Lago Fagnano is most likely promoted by cyclic rapid increases of sedimentation due to higher runoff and mass-wasting events. Increased runoff is related to the strength of the Southern Hemisphere Westerlies that, in turn, is modified by climate oscillations. Therefore, it is suggested that the cyclic repetition of the buried palaeo-redox fronts, showing periodicities of ~52 and ~4.5 years in the western and eastern sub-basins of Lago Fagnano, respectively, is forced by climate modes. The most likely candidates are the Antarctic Oscillation (AO) and the El Niño Southern Oscillation (ENSO), both impacting southernmost South America and showing similar sub-decadal modes and multi-decadal variations. Although the burial of redox fronts in lake or marine sediments is well-known, this study is the first to present a record of cyclic, high-frequency recurrence of these fronts most likely triggered by changing climate.

Keywords: Fe-/Mn-oxides; Redox fronts; Mixed lakes; Southernmost Patagonia; Palaeoclimate; Southern Hemisphere Westerlies

INTRODUCTION

The sensitivity of lakes to varying climatic conditions, stored in the lacustrine sedimentary record, is widely used in palaeoenvironmental studies (e.g., Bradley, 1999). However, the underlying processes leading to responses such as mixing or stratification remain complex and necessitate a thorough understanding of the lake physicochemical behaviour. Among others, the dynamics of redox fronts in time and space is a key process to understand different climatic forcing in lake systems. These fronts can migrate between the water column and the shallow sediment and affect biogeochemical cycling of organic matter and preservation of redox sensitive elements (Davison, 1993; Sobek *et al.*, 2009; Lau *et al.*, 2018). Seasonal cycles of precipitation, thermal gradients and wind intensity are factors that can trigger stratification, oxygenation or mixing that eventually changes the redox status of a lake. Moreover, increase in nutrients inputs may indirectly result in biological depletion of oxygen and subsequent changes in the redox status of water bodies (Davison, 1993). These events are seasonal but may also occur on a longer time-scale. Therefore, disentangling the forcing mechanisms responsible for these redox changes is necessary to understand the sedimentation and preservation processes in lacustrine archives prone for palaeoclimate studies.

Some redox-sensitive elements like Fe and Mn are preferentially used for such purpose (Davison, 1993; Bryant *et al.*, 1997). In palaeoclimate research, Fe and Mn profiles are commonly obtained from micro-X-ray fluorescence (μXRF) scanning of fresh surfaces of lake sediment cores (Davies *et al.*, 2015). In a well-mixed lake, the water column remains oxygenated at depth, and anaerobic conditions only prevail at the sediment-water interface or few centimetres below. In such reducing environment, the solubility of Fe and Mn increases, with Mn being far more soluble (Davison, 1993; Boyle, 2001; Burdige, 1993). Hence, an increase in sedimentary Fe/Mn ratios can point to the onset of anaerobic conditions due to stratification, or to de-oxygenation from organic decay following enhanced biological activity

(Davies *et al.*, 2015). The Mn/Fe ratio, on the other hand, is often used to trace bottom-water oxygenation (e.g., Francus *et al.*, 2013; Naeher *et al.*, 2013).

Various factors can influence the redox conditions in a lake, including changes in water depth, biological productivity, trophic state, and sedimentation rate. These changes can occur in response to changed climatic parameters such as temperature, precipitation and wind strength, and/or to anthropogenic impact. For instance, low Fe/Mn ratios at Lake Potrok Aike in Patagonia (Argentina) are suggested to result from increased lake mixing, either due to lake level lowering or enhanced wind speed (Haberzettl *et al.*, 2007). At Lake Montcortes in NE Spain, Fe/Mn ratios are proposed to reflect variations of agricultural runoff that modulate the biological productivity in the lake (Corella *et al.*, 2012). In Lake Baikal, Russia, sedimentary layers are enriched both in Mn and Fe, often forming crusts, and have been interpreted as formed during periods of reduced accumulation of suspended sediments at the transition between glacial and interglacial stages (Deike *et al.*, 1997; Granina *et al.*, 1993). These underlying factors controlling the Fe/Mn content in a lake are often ambiguous, requiring comprehensive multi-proxy approaches for unequivocal interpretation.

Lago Fagnano is the southernmost large ice-free lake outside Antarctica and, as such, a gateway for understanding past and present relations between Antarctic, South Pacific and South Atlantic climate changes. The sediments deposited in this lake during the Holocene underwent various sedimentological, geochemical and micropalaeontological analyses to reconstruct palaeoclimatic and environmental changes, glacier fluctuations and tectonic activity in this region (Waldmann *et al.*, 2008; 2010a; 2010b; 2011; 2014; Moy *et al.*, 2011). These studies demonstrate that the sediments deposited in Lago Fagnano are a sensitive and reliable recorder of past climate variability in the southern high latitudes. Strong Southern Hemisphere westerly winds impact Lago Fagnano, especially during austral summer causing lake mixing. The sediments exhibit a cyclic alternation of light clay and Fe-rich dark green to black laminae

throughout the Holocene. It has been suggested that they result from temporary oxygen depletion at the lake bottom under certain climate conditions (Waldmann *et al.*, 2010a). Nevertheless, the causes and frequency of the formation of these Fe laminae in Lago Fagnano are unknown, limiting further interpretation regarding changing redox conditions in the lake.

In this study, high-resolution sedimentological and geochemical data of sediment cores are presented to explain the mechanism of the Fe-rich laminae formation and preservation in the lake. Their composition, occurrence and frequency is analysed to identify the factors controlling their deposition and mechanisms behind changing patterns in redox conditions in Lago Fagnano during the Holocene.

REGIONAL AND LAKE SETTINGS

Lago Fagnano (54°S, ~68°W; 26 m asl) is located on the Tierra del Fuego archipelago in southernmost Patagonia (Fig. 1). The ca. 105 km E-W elongated and 10 km wide lake basin has evolved as a continental pull-apart structure that was deepened by subsequent Pleistocene glacial activity. The geology to the south and north of the lake is mainly composed of black shale and whitish-grey tuff sequences of the Sierras de Alvear, and marine greywacke of the Sierras de Beauvoir, respectively (Olivero and Martinioni, 2001; Tassone *et al.*, 2005). Large amounts of terrigenous elements, like Fe and Ti, are delivered to Lago Fagnano from weathering of these rocks by fluvial and aeolian influx (Gaiero *et al.*, 2003).

Lago Fagnano is divided into a smaller eastern sub-basin with a maximum water depth of 210 m and a larger, shallower western-central sub-basin of max. 130 m water depth (Fig. 1). The principal rivers flowing into the lake from the south and east are Río Milna, Río Valdez and Río Turbio, while only Río Claro drains into the central lake basin, coming from the north. One fluvial outlet, Río Azopardo, drains the lake at its westernmost extreme into the Almirantazgo Fjord (Admiralty Sound) towards the Strait of Magellan.

Owing to the harsh weather conditions in the region, information about the recent limnology of the lake is limited. The high water transparency, but low algal biomass and nutrient content indicate an ultra-oligotrophic to oligotrophic status (Waldmann *et al.*, 2014 and references therein). Further data collected in November 2006 revealed only small changes in pH (~7.8), temperature (~6°C) and oxygen content (~6-12 mg/l) in the water column and no significant thermocline establishment, which suggests well-mixed conditions during this early austral summer season (Waldmann *et al.*, 2014). Mixing and oxygenation of the water column was likely induced by heavy precipitation prevailing at that time and leading to a ~1.5 m higher than normal lake level (Waldmann *et al.*, 2014).

Climate in Tierra del Fuego is sub-polar, with moisture originating from the Pacific Ocean, in relation to the SE Pacific subtropical anticyclone and the circum-Antarctic low-pressure belt (Rogers and Loon, 1982). During austral summers, intense precipitation and increased zonal winds are forced by the Southern Hemisphere Westerlies (SHW) that migrate southwards to the region (Lamy *et al.*, 2001; Waldmann *et al.*, 2014). The cold and relatively drier austral winters are mostly influenced by the Antarctic Oscillation (AO) system (Gong and Wang, 1999).

MATERIAL AND METHODS

Sediment cores

The drilling campaign at Lago Fagnano was carried out in 2006 (Waldmann *et al.*, 2010a) and retrieved a series of 18 piston cores with up to 8 m length using a Kullenberg-type coring system. All cores were scanned at ETH Zürich, Switzerland, with a GEOTEK™ multi-sensor core logger (MSCL) to obtain their petrophysical properties (magnetic susceptibility, wet bulk density and P-wave velocity). For this study, sediment cores LF06-PC5 (126 m water depth) and LF06-PC17 (195 m water depth) were investigated from the western and eastern sub-basins of Lago Fagnano, respectively (Fig. 1B). These cores were retrieved in the vicinity of

previously studied seismic profiles and core sequences (Waldmann *et al.*, 2010a; Moy *et al.*, 2011). Core LF06-PC5 is 2.12 m long and presents grey and black sediment laminae in the upper 1.42 m, which represents the studied sequence in this contribution. The Hudson H1 tephra (7683 ± 33 ^{14}C yr BP; Stern *et al.*, 2016), identified as a ca. 3 cm thick deposit at 1.16 m depth in core LF06-PC5, is used as tephrochronological anchor. Core LF06-PC17 is 8.51 m long, with the lower 6.47 m containing slumped deposits, and the uppermost 2.04 m consisting of undisturbed and finely laminated sediments, and thus suitable to be used in this study. The core presents several event marker-layers that allowed a solid correlation to previously established event stratigraphy based on the nearby core LF06-PC16 (Figs. 1B and 2) (Waldmann *et al.*, 2011).

Radiocarbon dating

Previous attempts to establish age models for sediment cores from Lago Fagnano (LF06-PC12, -PC16 and -PC18; Fig. 1B) were based on the H1 tephra age (Stern, 2008; recently refined in Stern *et al.*, 2016) and Accelerator Mass Spectrometry (AMS) radiocarbon dating of bulk organic sediments, terrestrial macrofossils and pollen concentrates (Moy *et al.*, 2011; Waldmann *et al.*, 2011). The latter were found to produce the most reliable results for sediments from Lago Fagnano, whereas ages obtained from bulk sediments were 5000 to 7000 years older, most likely due to contamination with radiocarbon-dead material. The scarce terrestrial macrofossils that are mostly associated with mass-flow events are presumably redeposited from the basin slopes and produced too old ages as well (Moy *et al.*, 2011).

To obtain independent age models for the sediment cores investigated here, a total of six samples of pollen concentrates were prepared from the bottom, middle and top parts of the laminated intervals from cores LF06-PC5 and -PC17 (Table 1). Considering the low total organic carbon content (<1.2%) of Lago Fagnano sediments (Waldmann *et al.*, 2010a), and to assure that the minimum amount of carbon required for AMS dating can be extracted, relatively

7

thick (3-9 cm) slices of sediment were sampled. The extraction followed several physical and chemical separation steps mainly after Brown *et al.* (1989), Nakagawa *et al.* (1998), and Regnéll and Everitt (1996). The protocol included sieving with 250 and 6 μm meshes, treatment with heated HCl, KOH and H_2SO_4, and heavy-liquid density separation using CsCl and SPT (sodium polytungstate). After microscopic inspection of the remaining respective individual fractions, those containing mainly terrestrial organic micro-remains were merged and separation steps were repeated until no further purification was possible. AMS dating of the residual samples of organic micro-remains was done at the Poznan Radiocarbon Laboratory, Poland.

X-ray fluorescence element scanning and mapping

Continuous elemental composition of the sediment cores was determined by non-destructive micro-X-ray fluorescence (μ-XRF) scanning on the split-core sediment surface using an ITRAX elemental scanner (COX Analytical Systems; Croudace *et al.*, 2006) at the University of Bern, Switzerland. Both, a Cr-tube to capture variations of relatively lighter elements (Al, Si, S, K, Ca and Ti) and a Mo-tube for the proper detection of Mn and heavier elements (Fe, As, Rb, Sr and Zr) were applied, operated at 30 kV, 50 mA and 50 s exposure time per step. The relatively coarser lamination of core LF06-PC5 and the finely laminated sediments of LF06-PC17 were scanned in contiguous 1 and 0.5 mm increments, respectively. Element intensities are presented as centred log-ratios (clr = ln (element intensity / geometric mean of range of elements)) or log-element ratios to account for sediment-matrix and water-content effects (Tjallingii et al., 2007; Weltje and Tjallingii, 2008).

For high-resolution characterisation of the elemental distribution within the laminated sediments, elemental mapping of exemplary, ca. 1.5 x 1 cm sized areas was performed on impregnated and polished sediment blocks using an EAGLE III μ-XRF spectrometer (EDAX Inc.) at the University of Geneva, Switzerland. The device was employed with an Rh-tube operated with 40 kV voltage, 375 to 675 μA current, very short dwell times of 4 to 10 ms per

spot, and overlapping 50 μm spot sizes in ca. 24 μm steps. Elemental overlay images were produced using the EAGLE-internal evaluation software.

Scanning electron microscopy and X-ray diffraction analyses

Ten samples were taken from characteristic sediment laminae and dried for mineralogical analyses. Aliquots were ground and prepared for powder X-ray diffraction (XRD) analyses using a PANalytical-Empyrean X-ray diffractometer at the University of Geneva, Switzerland. A continuous scan mode was applied using Bragg-Brentano geometry, a step size of 0.013 °2θ and a counting time/step of 350 sec in the range of 4 to 70 °2θ with a Cu anode at 45 kV and 40 mA. Peaks were identified using the PANalytical HighScore Plus software.

For identification of different Fe and Mn phases in the sediments, ten aliquots were also inspected with a Jeol® JSM-7001 FA scanning electron microscope (SEM) at the University of Geneva, Switzerland, equipped with an energy dispersive X-ray analyser (EDS JED2300). After a first analysis, clay minerals were partially removed by centrifugation, allowing for improved observation of heavier fractions.

Thin section and image analysis

For microscopic inspection of different characteristics of laminated sediments along the analysed sediment cores, 20 petrographic thin sections of 10 cm length each were prepared at MKfactory (Germany). Standard protocols for thin section preparation of soft sediments were applied (e.g. Brauer *et al.*, 1999), including freeze-drying and impregnation with epoxy resin (Araldite 2020). Thin sections were investigated using a petrographic microscope with varying magnifications (25x to 400x) and optical conditions (plain parallel/semi-polarised/polarised light). Counting of dark laminae on core photographs was performed using the open-source software Strati-Signal (Ndiaye, 2007). Laminae were first identified semi-automatically via

alternating changes in greyscales and have then been corrected manually based on inspection of the core photographs and thin sections.

RESULTS

Sediment cores and age-depth models

Western-central basin core LF06-PC5

The 2.12 m long core LF06-PC5 is divided into two lithological units (LU1 and LU2; Fig. 3A). LU2 (2.12-1.42 m depth) is characterised by homogeneous, light grey clayey-silty mud, a relatively high density of ~1.8 g/cm³, and magnetic susceptibility values of ~20 x 10^{-5} SI. LU1 (1.42-0 m depth) presents alternating mm- to cm-scale, grey and black clayey-silt laminae and decreasing density and magnetic susceptibility towards the top of the unit. Five graded event layers of 1.5-19 cm thickness and a 3 cm thick tephra layer at 1.16 m depth are clearly identified by distinct high density and magnetic susceptibility values (Fig. 3A).

Radiocarbon ages retrieved from organic micro-remains revealed 10,870 ± 60 ^{14}C yr BP for the bottom, 6520 ± 70 ^{14}C yr BP for the middle, and 8220 ± 50 ^{14}C yr BP for the top of the laminated LU1 (Table 1; Fig. 3A). As these ages are considerably too old, the age model of core LF06-PC5 is, hence, based on linear inter- and extrapolation using the well-dated H1 tephra age (7683 ± 33 ^{14}C yr BP; Stern *et al.*, 2016), calibrated to 8469 ± 39 yr BP. Following this approach, the laminated LU1 of core LF06-PC5 was deposited during the last ~10,900 years (Fig. 3A).

Eastern basin core LF06-PC17

The upper 2.04 m of core LF06-PC17 (Fig. 3B) present undisturbed alternations of mm-scaled black and grey, clayey-silty laminae with relatively constant density (1.3-1.5 g/cm³) and magnetic susceptibility (10-12 x 10^{-5} SI) values that are comparable to those measured in LU1 of LF06-PC5 (Fig. 3A). Six graded event layers of 0.5 to 12.5 cm thickness have been identified

by elevated density and magnetic susceptibility values. These clastic layers are typically characterised by a dark grey, coarse silty to sandy base followed by upward fining and a whitish clay top and have been interpreted as mass-transport deposits triggered by earthquakes (Waldmann *et al.*, 2011).

Similar to the western basin, radiocarbon dating of organic micro-remains from the bottom, middle and top parts of the undisturbed laminated top-section of core LF06-PC17 (Fig. 3B) resulted in too old ages (Table 1). The accurate transfer of published ^{14}C ages obtained from core LF06-PC18 (Fig. 1; Moy *et al.*, 2011) to this core was escorted by large caveats in the proper correlation. Therefore, the age model for core LF06-PC17 is based on correlating the event stratigraphy with the published record from core LF06-PC16 by Waldmann *et al.* (2011) (Fig. 2). Furthermore, this correlation approach was extended to core LF06-PC14, as there is no accurate age for the bottommost event in core LF06-PC16 (C16; Waldmann *et al.*, 2011) (Fig. 2). Linear interpolation between events C18 and C15 resulted in an age estimate of 3311 yr BP for event C16, which is equivalent to event #17-6 in core LF06-PC17. Hence, the bottom of the laminated section of core LF06-PC17 can be estimated with such an age. A constant sedimentation rate of ~0.52 mm/year is calculated for core LF06-PC17, when event layers are extracted and considering them as non-erosive.

Sediment composition and elemental characteristics

Sediments of both investigated cores are predominantly clastic and composed of clay and silt, as well as fragmented and mostly centric diatoms (of the genus *Discostella*; Waldmann *et al.*, 2014). XRD and SEM analyses reveal a monotonous and similar composition for both cores, regardless of the presence of laminae or other structures. It is characterized by illite-type clay minerals, quartz, albite (plagioclase feldspar) and chlorite (phyllosilicates). Birnessite (Mn-oxide) and Fe-oxide were detected in the top 5 cm of core LF06-PC5 by both XRD and SEM. These oxides appear as amorphous, ca. 5-15 µm sized conglomerated sheets (Fig. 4).

The XRF elemental composition greatly resembles the homogeneous lithology along the laminated parts of the core profiles (respective LU1 in cores LF06-PC5 and -PC17; Fig. 3). Varying intensities of the elements for which centred log-ratios were calculated (Al, Si, S, K, Ca, Ti, Mn, Fe, As, Rb, Sr and Zr) are mainly associated with the occurrence of mass-transported deposits and the pattern of light and dark laminations. Fe is by far the dominant element, showing four-fold higher counts than the geometric mean of the considered elements. Lowest counts were recorded for S and As (Fig. 3).

After extraction of the event layers from the XRF profiles in cores LF06-PC5 and -PC17, principal component analysis (PCA) was applied to the normalized data, as well as to the element-ratios Fe/K, Mn/K, Mn/Fe, and the incoherent (Compton) / coherent (Rayleigh) scattering ratio of the XRF device (inc/coh ratio) retrieved from the Mo- and Cr-tube, respectively (Fig. 5). For both cores, the first two principal components (PC1 and PC2) explain about 60% of the observed variance in the XRF data. Considering also correlation coefficients (Table 2), the regarded elements and ratios describe two main inter-relations:

(1) PC1 shows an anti-relation between elements that are bound to minerogenic detritus (Al, Si, K, Ca, Ti, Rb, Sr and Zr, related to clay minerals, quartz, and feldspars; red in Fig. 5) and parameters that are associated with sediment components built in the lake. To discriminate between potential authigenic/diagenetic and detrital Fe- and Mn- phases, these two elements were normalized against K, which shows the best counting and correlation values amongst the allogenic elements. Fe/K and Mn/K correlate well (R ≥ 0.89) with Fe and Mn, respectively, implying the dominance of authigenic or diagenetic phases in the sedimentary record. Only in the western-basin core LF06-PC5, a slightly weaker correlation between Fe/K and Fe (R = 0.71), as well as an insensitivity of Fe to reflect the first principal component (Fig. 5) are observed, indicating the presence of some detrital Fe-phases. The positive correlation of S and As with Fe/K in both sediment cores points

towards their common binding within Fe-sulphide. Furthermore, Fe/K, S and As correlate well with the incoherent/coherent scattering ratio, which resembles the average atomic number of the sediment matrix composition. Since organic carbon has a lower atomic number than the measurable elements, this ratio can be used as a qualitative estimation of the organic content of the sediment (e.g., Burnett *et al.*, 2011).

(2) The second principal component (PC2) describes the relation between sedimentary Fe (associated with S, As and inc/coh) and Mn (Fig. 5) that are susceptible to changing reducing or oxidising (redox) conditions. The Mn/Fe ratio, which indicates oxidation, shows a slight anti-correlation with Fe/K (Table 2).

Characterisation of the sediment lamination

The light-dark lamination patterns observed in the sediment cores of Lago Fagnano were inspected by thin section microscopy, and µXRF elemental scanning and mapping. The lamination patterns found in the two sub-basins show overall similar sedimentary and elemental characteristics, but distinctly different laminae thicknesses (Figs. 6 and 7).

Coarse lamination in the western-central sub-basin

Core LF06-PC5 presents a continuous, few mm- to cm-scaled lamination pattern of black and greenish clay layers embedded within the light grey clayey-silty background sediments (Fig. 6). The grey sediment is dominantly composed of clastics, which is reflected in elevated XRF values of detrital elements (represented by K in Fig. 6A). A second main component of the light grey mud is Mn that reaches highest values in the topmost ~2 cm of the core (Fig. 6A). There, birnessite, a layered manganese oxide, was detected by XRD and SEM (Fig. 4) and is observed as dark brown to black patches (Fig. 6B). Further down-core, these patchy Mn-oxide accumulations are still visible in thin sections and the XRF maps within the light grey sediment matrix, but not on the split-core surface (Fig. 6C).

Black laminae are often discontinuous and their colour rapidly fades after core opening, *i.e.* after exposing the sediment to oxygen. In the thin sections, black laminae appear faint and particularly fine-grained, building a hardly recognizable contrast to the clayey matrix sediment (Fig. 6C). These laminae show distinct positive peaks in Fe, As, S and coh/inc, and negative excursions of Mn and K (like all other detrital elements; Fig. 6A). The most pronounced Fe-peaks are, however, observed within three orange-brown layers at ca. 2.5-5 cm depth (Fig. 6B) that underlie the Mn-enriched brownish patches at the top of the core, and in occasional greenish laminae (Fig. 6C). Dark, *i.e.* black or greenish laminae appear on average every ca. 5 mm.

Fine lamination in the eastern sub-basin

A fine, mm-scaled lamination is observed in core LF06-PC17 (eastern sub-basin; Fig. 7). Like in the western-central sub-basin, the lamination pattern consists of fine-grained and faint black and greenish laminae, yet their frequency is higher (every ca. 2 mm). The elemental distribution within the laminae in core LF06-PC17 is comparable to that of the western basin, with detrital elements (e.g. K; Fig. 7A) and Mn/Fe being enriched in the light grey clayey-silty sediment, and peaks of Fe, As, S and coh/inc in the thin black and greenish laminae. A different behaviour is observed for greenish laminae preceding mass-transport deposits, where Fe and Mn are enriched and S is depleted (Fig. 7A and B). The enrichment of Mn, Fe and As within black-brownish Mn- and orange-brownish Fe-oxide layers at the top of the western-basin (core LF06-PC5; Figs. 3 and 6) is not detected in core LF06-PC17. However, in the eastern-basin core LF06-PC16, a fragment of such orange-brown layer is observed at ca. 2.5 cm depth, at the top of the mass-transport event C24 (*i.e.* event #17-1 in core PC17; Fig. 2). This Mn-Fe-enriched layer was likely eroded in PC17 by the mass-wasting event.

Frequencies of Fe/Mn laminae

Black and greenish Fe-laminae were identified and counted based on their visual appearance in core and thin section images, and greyscale values of the core photographs. Changing frequencies of these laminae were then calculated using the linear age-depth relationship established for the two sediment cores.

In the western-basin (core LF06-PC5), a total of 211 dark laminae was counted within the 1.425 m long section (LU1; Fig. 3A). Extracting event layers from the profile and assuming a basal age of 10,910 cal. yr BP (event #5-4 in Fig. 3A) results in an event-free length of 1.17 m of the laminated section, an estimated sedimentation rate of 0.11 mm/year, and an average laminae frequency of 52 years. This ca. 50-year frequency is observed during most of the investigated time-interval (Fig. 8A), from ca. 600 to 7100 cal. yr BP and from ca. 9400 to 10,900 cal. yr BP, where values fluctuate between ca. 20 and 80 years. In the topmost ca. 7 cm (recent (= 2006 AD) to ca. 600 cal. yr BP), only three orange-brownish layers and one faint black lamina are observed. Between ca. 7100 and 9400 cal. yr BP, the recurrence interval of dark laminae increases to average values of ca. 80 and maximum values of up to 250 years (Fig. 8A).

The undisturbed laminated section of the eastern-basin core LF06-PC17 (0-2.04 m sediment depth; Fig. 3B) contains a total of 756 black and greenish laminae. Accepting an age of 3310 cal. yr BP (Fig. 3B) and an event-corrected depth of 1.76 m for the base of the laminated section leads to an estimated sedimentation rate of 0.52 mm/yr and an average laminae frequency of 4.5 years. The periodicity of laminae varies between ca. 1 and 16 years (Fig. 8B). More frequent laminae, on average every 3.3 years, are observed during the last ca. 600 years. Between ca. 1800 and 2850 cal. yr BP, the rate of laminae frequency is slightly elevated to 5.3 years on average due to some peaks of up to 16 years (Fig. 8B).

DISCUSSION

Age model construction

Radiocarbon-'dead' lignite (coal) present in mudstones within the catchment of Lago Fagnano contaminates the lacustrine dissolved inorganic carbon (DIC) pool, and therefore limits the reliable radiocarbon dating of the lake sediments (Moy *et al.*, 2011; and references therein). By comparing radiocarbon ages of bulk organic sediments, terrestrial macrofossils and pollen concentrates from the eastern-basin core LF06-PC18 (Fig. 2), Moy *et al.* (2011) identified a 5000 to 7000 cal. yr offset of bulk organic ages to corresponding pollen dates. Similarly, terrestrial macrofossils produced too old ages, most likely due to remobilization from the basin slopes. Due to the isotopic equilibrium of trees and pollen with the atmospheric radiocarbon pool, therefore, dating of pollen concentrates produced the most accurate Holocene chronology for Lago Fagnano with a minimum error estimate of less than 300 cal. yr (Moy *et al.*, 2011). However, despite applying a similar protocol for pollen extraction as in Moy *et al.* (2011), in the six samples from the LF06-PC5 and LF06-PC17 cores analysed here, relative pollen amounts of only 10 to 60% could be obtained (Table 1). Significant proportions of non-pollen organic micro-remains, *i.e.* plant tissues, charred particles, algae and fungal residues (Table 1), likely contaminate these samples with old carbon. Thereby, the ^{14}C-depleted carbon is incorporated in aquatic plants from the lake DIC pool that can have received old DIC from groundwater or the bedrock (e.g., Abbott and Stafford, 1996; Albéric *et al.*, 2016). The high amount of charred particles (20-50%) in the samples suggests that erosion and influx of old particulate organic carbon from peats, soils and the coal-bearing bedrock of the drainage basin to the lake is a further, probably even more important source of contamination. Consequently, radiocarbon ages of all six samples turned out to be implausible, showing offsets of ca. 2000 to 12,000 cal. yr to the corresponding expected ages based on the H1 Hudson tephra (Stern *et al.*, 2016) and event-layer correlation (Waldmann *et al.*, 2011) (Table 1; Figs. 2 and 3).

Therefore, linear age-depth models were established here for both investigated sediment cores following the approach of Waldmann *et al.* (2010a); (2011). The H1 Hudson tephra age

(calibrated to 8469 ± 39 cal. yr BP) is well constrained by ^{14}C dating in numerous outcrops, peat bogs and lakes in the region, where no freshwater reservoir effects were encountered (Stern, 2008; Stern *et al.*, 2016). This chronostratigraphic anchor provides the only available independent age control for Lago Fagnano sediments. The assumption of constant sedimentation rates in the two sub-basins of Lago Fagnano during the Holocene is justified, since no significant long-term trends or changes in the XRF profiles of detrital elements (e.g., K and Ti in Fig. 3) and in grain size are observed in the laminated sediments. The event stratigraphy correlated between cores LF06-PC17 (this study) and LF06-PC16 (Waldmann *et al.*, 2011) is unequivocal (Fig. 2). Transferring the published pollen ages of core LF06-PC18 (Moy *et al.*, 2011; Fig. 2) to core -PC17, however, reveals an offset of the pollen dates of ca. 400 to 700 cal. yr to the event-derived estimations. This offset is close to the reported average ~300 yr error of pollen ages (Moy *et al.*, 2011), but it may also indicate a delayed deposition of pollen in the sediments or slight contamination of these samples. Hence, the chronologies of the investigated cores are considered to be reliable, even though further independent absolute age control is still missing.

Lago Fagnano sediment record

XRF element scanning of lacustrine sediment cores is a valuable and widely used tool to characterise lithological changes through time, and decipher underlying catchment-related and lake-internal processes (see e.g. various contributions in Croudace and Rothwell, 2015). Supported by PCA, thin section microscopy, XRD and SEM analyses, the following inferences are drawn from the XRF dataset of the Lago Fagnano sediment cores under focus in this study:

The overall homogeneous grain size and clastic composition of the light grey clayey-silty mud, as reflected in XRF logs (Fig. 3), implies a stable long-term supply of detrital sediments to Lago Fagnano during the Holocene. Clastic sediments are predominantly delivered by fluvial runoff, which in turn controls the sediment accumulation rates in the lake. In previous studies, the Fe

content in Lago Fagnano sediments was interpreted as an indirect proxy for precipitation (Waldmann *et al.*, 2010a). However, the PCA of XRF data from cores LF06-PC5 and -PC17 (Fig. 5) demonstrates a diagenetic alteration of Fe. Therefore, lithogenic elements that are inert to early diagenetic processes, *i.e.* Al, Si, K, Ti, Rb or Zr (Davies *et al.*, 2015), are more appropriate to use as indicator for precipitation changes at Lago Fagnano.

The constant slight decrease of Al, Si and K, *i.e.* elements indicative for clay minerals, along with declining density (Fig. 3A) may be related either to diminishing influx of suspended particles from glacial meltwater or to the development of vegetation and soils during the Holocene leading to reduced erosion from the catchment. The latter would be supported by palynology, reporting the progressive establishment of *Nothofagus* forest in the Fagnano watershed (Waldmann *et al.*, 2014). This is accompanied by the overall increasing trend of lake productivity and nutrient supply to Lago Fagnano during the Holocene, shown e.g. by bulk organic C and N curves (Waldmann *et al.*, 2010a; Moy *et al.*, 2011). The S and inc/coh logs of core LF06-PC5 (Fig. 3) redraw this increasing trend during the studied time interval, which suggests a correlation with the organic carbon content of the sediments. Indeed, S is related to enriched organic matter (e.g., Passier *et al.*, 1999; Thomson *et al.*, 2006), and the XRF inc/coh scattering ratio has been shown to be a useful proxy for the organic content of sediments (Burnett *et al.*, 2011).

Formation and preservation of Fe/Mn-laminae

Waldmann *et al.* (2014) suggested that the cyclic alternation of light-grey clay and black/greenish laminae indicate their sedimentation in a well-stratified lake, which might have induced anoxic or dysoxic conditions at the sediment-water interface. Fluctuations of redox-sensitive elements in the XRF data, where detrital elements and Mn/Fe are enriched in the light grey sediment, while Fe/K, S and As peaks depict black and greenish laminae (Figs. 6 and 7), confirm that laminae formation in Lago Fagnano is related to redox processes. In the following

paragraphs are explained in detail the early diagenetic processes, *i.e.* the formation, burial, and subsequent partial dissolution and pyritisation of redox boundaries, leading to laminae formation and preservation in Lago Fagnano.

The active redox front

The orange-brown Fe-oxide layers and brownish-black Mn-oxide patches, detected in the top ~5 cm of the western-basin core LF06-PC5 (Fig. 6), are interpreted to have formed at the active redox front (Fig. 9A). Such redox boundary develops, when dissolved Mn(II) and Fe(II) diffuse upwards within reduced sediments and oxidise to Mn(IV) and Fe(III) as soon as the O_2 concentration gets sufficient (e.g., Davison, 1993; Torres *et al.*, 2014). As the dark-brownish Mn-oxide accumulations are located in the top-most sediments, it can be assumed that O_2 penetration into the sediments is restricted, and that the oxic-anoxic interface is positioned at the water-sediment boundary in Lago Fagnano. Mn(II) is more soluble than Fe(II) and, hence, O_2 from the water column is consumed to build MnO_2, whereas Fe(II) is oxidised from Mn(IV) leading to Mn reduction and the accumulation of an Fe-oxide layer right underneath the Mn-enriched layer (e.g., Och *et al.*, 2012). Arsenic, strongly enhanced within the Fe-oxide layer (Fig. 6), is likely affected by similar post-depositional diagenetic remobilisation processes (Farmer and Lovell, 1986). Under oligotrophic conditions, deep oxygenation of the hypolimnion, and constantly low sediment accumulation rates, this Fe/Mn-oxide layer will dynamically grow and move upwards with sedimentation, following the water-sediment redox interface. A change of these conditions can induce the burial of the Fe/Mn-oxide accumulation into deeper sediments and a subsequent initiation of a new dynamic Fe/Mn-layer at the re-established O_2-Mn(II) interface (e.g., Granina *et al.*, 2004; Och *et al.*, 2012; Torres *et al.*, 2014).

Such sedimentary Fe/Mn-redox fronts have been described from other oligotrophic and well-ventilated deep lacustrine and marine environments comparable to Lago Fagnano, for instance the central Arctic Ocean (März *et al.*, 2011; Löwemark *et al.*, 2014), equatorial upwelling

systems in the Atlantic and Pacific oceans (e.g., Burdige, 1993), Lake Ohrid in Albania/Macedonia (Vogel *et al.*, 2010), Loch Lomond in Scotland (e.g., Farmer, 1994), and particularly Lake Baikal, where these active and buried Fe/Mn-layers have been extensively studied (e.g., Granina *et al.*, 1993; 2004; 2010; 2011; Deike *et al.*, 1997; Müller *et al.*, 2002; Och *et al.*, 2012; Torres *et al.*, 2014).

Potential mechanisms behind Fe/Mn-redox front burial

Several mechanisms may hinder the diffusive oxygen flux from the water column to the sediment and thus cause the surface Fe/Mn-layer burial (e.g., Granina *et al.*, 2004; Och *et al.*, 2012; Torres *et al.*, 2014):

- Enhanced mass accumulation rate of settling organic matter, due to higher biological productivity and/or increased influx, would lead to stronger oxygen consumption in the sediment. Floods carrying high amounts of organic matter were suggested to trigger this mechanism in Lake Storsjön (Sweden), where black organic-rich layers were preserved in the sediments that are enriched in Fe sulphides (Labuhn *et al.*, 2018). In Lago Fagnano, peaks in the inc/coh ratio from XRF data (Figs. 6 and 7) in correspondence to Fe-rich layers indeed suggest a slightly higher organic carbon content in these (palaeo-) redox fronts. However, as the overall TOC content of <1.2% (Waldmann *et al.*, 2010a) is very low, this mechanism to bury redox fronts is considered as insignificant here.

- Stratification of the water column, caused e.g. by changes in wind strength, temperature, lake level, and/or aquatic productivity, would decrease the bottom water oxygen concentration. Seasonal mixing and stratification is the main driver for the formation and preservation of annual laminations in many lakes, e.g. in oligotrophic Swedish lakes, where seasonal precipitation of Fe hydroxides and sulphides leads to characteristic colour-banding of the varved sediments (e.g., Renberg, 1986; Shchukarev *et al.*, 2008; Gälman *et al.*, 2009). A further example, but on multi-millennial time-scales, are sapropels in the

Mediterranean Sea. Sapropels are layers enriched in organic carbon and redox-sensitive elements that were formed due to amplified runoff from North Africa through the Nile River during past orbital summer insolation maxima, resulting in anoxia of the deep East Mediterranean Sea (e.g., Thomson *et al.*, 2006; Rohling *et al.*, 2015, and references therein). In the case of Lago Fagnano, episodic stratification promoted by changing wind regime can possibly explain burial phases of redox fronts. However, stratification was not observed in the lake, and the presence of broken littoral diatom frustules throughout the light and dark sediment layers in the deep basins (Waldmann, 2008; Waldmann *et al.*, 2014) indicates recycling of sediments from shallow areas of the lake due to persisting wind-driven wave activity and mixing.

- An increase in sedimentation rate would lead to a larger diffusive pathway and separate the O_2–Mn(II) interface. Granina *et al.* (2004) suggested that Fe/Mn-layers in Lake Baikal sediments can be used as a proxy for periods of low sedimentation rates and well-oxygenated conditions, and that these redox fronts were buried by rapid changes in sedimentation regime. The same mechanism was proposed for concretionary Fe/Mn-horizons observed in Lake Ohrid sediments (Vogel *et al.*, 2010). At both, Lake Baikal and Lake Ohrid, lake conditions under which these redox fronts form and preserve are comparable to Lago Fagnano, *i.e.* a deep-water, oligotrophic, well-mixed setting with generally low productivity and sedimentation rates. The particularly well preserved redox fronts underlying mass-wasting events in Lago Fagnano (Fig. 7) confirm that a rapid increase in sedimentation is a plausible mechanism to explain buried Fe/Mn-laminae also here.

- Burial might also result from a steady-state process of increasingly slowed down, and at some point limited reductive dissolution when the active Fe/Mn-layer grows. Och *et al.* (2012) suggested this mechanism as an alternative explanation for the cyclic pattern of Fe/Mn-layers in Lake Baikal. They proposed that a new active front evolves at the

O_2/Mn(II) redox boundary along with the burial of the old Fe/Mn layer, which then slowly dissolves and feeds the new redox boundary. This process cannot be ruled out as explanation for the burial of Fe/Mn-layers, and is not related to singular, potentially climate-driven events, in contrast to the mechanisms illustrated above.

Partial dissolution and pyritisation of buried Fe/Mn-laminae

Although clear Mn-laminae can be distinguished at the top of the core (Fig. 6B), they are rarely found as proper laminae down-core, and rather occur as patchy enrichments (Fig. 6C). A similar pattern is observed for Fe-layers in the deeper parts of the core, where Fe-oxide laminae are only sporadically preserved, except under turbidite layers. These Fe-rich discontinuous layers are often enriched in S and As. This is uniquely observed under XRF and µXRF scans. Arsenic being strongly incorporated into FeS_2 (Peterson and Carpenter, 1986; Huerta-Diaz and Morse, 1992), this enrichment suggests the presence of mineralized sulphide phases. However, no XRD or SEM data could confirm the presence of pyrite. Instead, quick fainting of black laminae after oxygen exposure upon core opening suggest rapid oxidation of unstable Fe-sulphide phases like mackinawite or greigite that are precursors of pyrite.

This Fe-loss is likely the result of continued microbial activity down-core. Namely, bacterial sulphate reduction is responsible for the production of sulphide that subsequently reduces Fe-phases and leads to the partial dissolution of Fe-oxide laminae and the formation of Fe-S minerals through the reaction of Fe^{2+} and sulphides (e.g., Berner, 1970, 1984; 1985; Burdige, 1993) (Fig. 9B). The absence of pyrite however indicates that the sulphidisation of the sediments is limited, and rather results in the partial pyritisation and preservation of intermediate phases (Richter *et al.*, 2006). In oligotrophic lacustrine environments, and particularly in Lago Fagnano, where sulphate is depleted, the relatively limited amount of primary production associated to low sulphate levels may be the limiting factor for sulphate reduction activity (Berner, 1984; Holmer and Storkholm, 2001). Therefore, although Fe^{2+} is

available (likely remobilized by iron reducing organisms), the absence of sulphide or sulphate in general prevents complete pyritisation of the sediment.

Excess ferrous Fe that cannot react with sulphide may diffuse away and reduce manganese oxides as suggested by Och *et al.* (2012) in Lake Baikal, resulting in the associated loss of Mn down-core. In sulphide-depleted sediments, processes like methanogenesis become prevalent and allow for the formation and preservation of phosphate minerals like vivianite (Berner, 1981; Manning *et al.*, 1999). Here, vivianite could not be detected under SEM or XRD. Visual inspection of the core showed blue spots interpreted as vivianite within gravity events only. Phosphorus could not be investigated further as it remained below detection limit all along the core. Overall, sampling could not be renewed recently and a thorough study of active microbial communities and biogeochemical cycles will be needed to validate controlling factors over Fe/Mn-lamina dissolution and preservation.

Potential climatic forcing of cyclic redox front burial

The ultimate trigger for the burial of Fe/Mn-redox fronts in the sediments of Lago Fagnano cannot be unequivocally determined by the approach applied here. However, the cyclic appearance of these laminae with periodicities similar to climate oscillations is intriguing. Following this argumentation, rapid and recurrent increase in sedimentation rates is suggested as the most likely mechanism behind the burial of Fe/Mn-laminae in Lago Fagnano. Enhanced sediment influx is forced by higher runoff related to increased precipitation in the lake's watershed (Waldmann *et al.*, 2010a). Moreover, wind strength and rainfall amounts in Tierra del Fuego are mostly controlled by the Southern Hemisphere Westerlies, which in turn are modulated by the El Niño Southern Oscillation (ENSO) and the Antarctic Oscillation (AO) on inter-annual and decadal timescales (e.g., Garreaud *et al.*, 2009; Pohl *et al.*, 2010).

The dominant influence of inter-annual and decadal-scale variations of ENSO on climate variability in the Americas is well documented for the observational period (Dettinger *et al.*,

2001). Thereby, a reduction of ENSO activity in the 2–3-yr periodicity range during the period 1920–60, compared with earlier and later periods, emphasizes strong multi-decadal variations of ENSO over the past century (Kestin *et al.*, 1998). The influence of ENSO on climate in southern South America beyond the instrumental record has also been reported from Patagonian lake records. For example, in the proglacial Lago Frías at 40°S, the thickness of clastic-organic varves that formed during the last ca. 280 years has been suggested to be controlled predominantly by ENSO (Ariztegui *et al.*, 2007), which was also proposed for wind-induced varve thickness changes in Lago Puyehue (40°S) sediments during the last ca. 600 years (Boës and Fagel, 2008).

Besides ENSO, the Antarctic Oscillation has also played a significant role in modulating the low-frequency variability of precipitation in southern South America (Silvestri and Vera, 2003). Villalba *et al.* (1997) proposed that cyclonic activity was stronger in the mid-twentieth century than previously in the South American sector of the Southern Ocean. The 3.3 yr cyclicity of sediment lamination obtained from Lago Fagnano core LF06-PC17 for the last ca. 600 years (Fig. 8B) agrees well with Villalba *et al.*'s (1997) reconstruction of Southern Ocean sea-level pressure expressing the AO, based on South American subantarctic tree ring records since 1750 AD.

The average frequencies of Fe/Mn-laminae of 4.5 and 52 years in the eastern and western sub-basins of Lago Fagnano, respectively, fall well in the range of both, the 2-8 year periodicities of ENSO and the AO, including their reported multi-decadal variations. Yet, there is no clear explanation why inter-annual cycles are only reflected in the deeper eastern sub-basin, while in the shallower western sub-basin of Lago Fagnano laminations are preserved only on multi-decadal time-scales. It is reasonable to assume that these different periodicities are related to the specific conditions characterising each sub-basin (e.g., dissimilar water depths and number of tributaries contributing suspended sediments). Therefore, changes in the Southern

Hemisphere westerlies strength and precipitation would affect the ventilation and sediment accumulation rates in the two sub-basins differently. However, the question remains open, as the Lago Fagnano lamination might be triggered by these oscillations or by a process that is not climatically driven (Och *et al.*, 2012). Furthermore, the present chronology prevents from proper interpretation and correlation to instrumental records of ENSO and AO. Similar radiocarbon dating problems due to the presence of radiocarbon-dead lignite have been previously noted in other sites in Patagonia (Ariztegui *et al.*, 2007). Thus, a better climate discussion for the region could only be done using varved lake sediments or tree ring records that are, however, so far not available in the area. Analogously, obtaining an independent age control, for example from further tephra time markers, would be much helpful.

CONCLUSIONS

The Holocene sedimentary record of Lago Fagnano in Tierra del Fuego contains a continuous lamination pattern despite deep ventilation of the water column, which is forced by year-round prevailing strong Southern Hemisphere Westerly winds that would inhibit the preservation of these fine layers. Applying high-resolution sediment-geochemical analyses allowed deciphering the mechanisms, frequencies, and potential climatic forcing of laminae formation and preservation in Lago Fagnano. The fine black and greenish laminae within predominantly clastic sediments show distinct fluctuations of redox-sensitive elements, *i.e.* Fe, Mn, S and As, which led to the assumption that these laminae are the remnants of palaeo-oxidation fronts. From potentially four mechanisms that can explain the burial of such redox fronts in a sedimentary record, a rapid increase of sedimentation rates is the most likely mechanism for the oligotrophic and well-mixed Lago Fagnano. This is supported by particularly well-preserved Fe/Mn-layers underlying mass-transported deposits. After their burial, early diagenetic processes affected these Fe/Mn-layers through partial dissolution and pyritisation, involving complex biogeochemical element cycling.

These processes related to changing redox conditions and the preservation/diagenesis of sedimentary Fe/Mn-layers in Lago Fagnano might well serve as an analogue for buried redox fronts in similar oligotrophic, deep-water, and deeply oxygenated lacustrine and marine settings. Moreover, such high-frequency, sub-decadal recurrence of buried palaeo-oxidation fronts in a sediment record have never been described before. The cyclic rapid increases in sedimentation rates are proposed to be related to changed runoff to the lake, controlled by the strength of the Southern Hemisphere Westerlies that is modified by ENSO and AO on multi- and sub-decadal time-scales. This study, therefore, demonstrates the great value of the Lago Fagnano sedimentary record as a climate archive.

ACKNOWLEDGEMENTS

REFERENCES

Abbott, M.B. and Stafford, T.W. (1996) Radiocarbon Geochemistry of Modern and Ancient Arctic Lake Systems, Baffin Island, Canada. *Quat. Res.*, **45,** 300-311.

Albéric, P., Jézéquel, D., Bergonzini, L., Chapron, E., Viollier, E., Massault, M. and Michard, G. (2016) Carbon Cycling and Organic Radiocarbon Reservoir Effect in a Meromictic Crater Lake (Lac Pavin, Puy-de-Dôme, France). *Radiocarbon*, **55,** 1029-1042.

Ariztegui, D., Bösch, P. and Davaud, E. (2007) Dominant ENSO frequencies during the Little Ice Age in Northern Patagonia: The varved record of proglacial Lago Frías, Argentina. *Quat. Int.*, **161,** 46-55.

Berner, R.A. (1970) Sedimentary pyrite formation. *Am. J. Sci.*, **268,** 1-23.

Berner, R.A. (1981) A new geochemical classification of sedimentary environments. *J. Sediment. Res.*, **51,** 359-365.

Berner, R.A. (1984) Sedimentary pyrite formation: An update. *Geochim. Cosmochim. Acta*, **48,** 605-615.

Berner, R.A. (1985) Sulphate reduction, organic matter decomposition and pyrite formation. *Philosophical Transactions of the Royal Society of London. Series A, Mathematical and Physical Sciences*, **315,** 25-38.

Boës, X. and Fagel, N. (2008) Relationships between southern Chilean varved lake sediments, precipitation and ENSO for the last 600 years. *J. Paleolimnol.*, **39,** 237-252.

Boyle, J.F. (2001) Inorganic Geochemical Methods in Palaeolimnology. In: *Tracking Environmental Change Using Lake Sediments* (Eds W. Last and J. Smol), *Developments in Paleoenvironmental Research*, **2**, pp. 83-141. Springer Netherlands.

Bradley, R.S. (1999) *Paleclimatology - Climates of the Quaternary*. Elsevier Academic Press.

Brauer, A., Endres, C. and Negendank, J.F.W. (1999) Lateglacial calendar year chronology based on annually laminated sediments from Lake Meerfelder Maar, Germany. *Quat. Int.*, **61,** 17-25.

Brown, T.A., Nelson, D.E., Mathewes, R.W., Vogel, J.S. and Southon, J.R. (1989) Radiocarbon dating of pollen by accelerator mass spectrometry. *Quat. Res.*, **32,** 205-212.

Bryant, C.L., Farmer, J.G., MacKenzie, A.B., Bailey-Watts, A.E. and Kirika, A. (1997) Manganese behavior in the sediments of diverse Scottish freshwater lochs. *Limnol. Oceanogr.*, **42,** 918-929.

Burdige, D.J. (1993) The biogeochemistry of manganese and iron reduction in marine sediments. *Earth-Sci. Rev.*, **35,** 249-284.

Burnett, A.P., Soreghan, M.J., Scholz, C.A. and Brown, E.T. (2011) Tropical East African climate change and its relation to global climate: A record from Lake Tanganyika, Tropical East Africa, over the past 90+kyr. *Palaeogeog. Palaeoclimatol. Palaeoecol.*, **303,** 155-167.

Corella, J.P., Brauer, A., Mangili, C., Rull, V., Vegas-Vilarrúbia, T., Morellón, M. and Valero-Garcés, B.L. (2012) The 1.5-ka varved record of Lake Montcortès (southern Pyrenees, NE Spain). *Quat. Res.*, **78,** 323-332.

Croudace, I.W., Rindby, A. and Rothwell, R.G. (2006) ITRAX: description and evaluation of a new multi-function X-ray core scanner. *Geological Society, London, Special Publications*, **267,** 51-63.

Croudace, I.W. and Rothwell, R.G. (2015) *Micro-XRF Studies of Sediment Cores: Applications of a non-destructive tool for the environmental sciences*. Springer Science, Dordrecht, 688 pp.

Davies, S.J., Lamb, H.F. and Roberts, S.J. (2015) Micro-XRF Core Scanning in Palaeolimnology: Recent Developments. In: *Micro-XRF Studies of Sediment Cores* (Eds I.W. Croudace and R.G. Rothwell), *Developments in Paleoenvironmental Research*, **17**, pp. 189-226. Springer Netherlands.

Davison, W. (1993) Iron and manganese in lakes. *Earth-Sci. Rev.*, **34,** 119-163.

Deike, R.G., Granina, L., Callender, E. and McGee, J.J. (1997) Formation of ferric iron crusts in Quaternary sediments of Lake Baikal, Russia, and implications for paleoclimate. *Mar. Geol.*, **139,** 21-46.

Dettinger, M.D., Battisti, D.S., Garreaud, R.D., McCabe, G.J. and Bitz, C.M. (2001) Chapter 1 - Interhemispheric Effects of Interannual and Decadal ENSO-Like Climate Variations on the Americas. In: *Interhemispheric Climate Linkages* (Ed V. Markgraf), pp. 1-16. Academic Press, San Diego.

Farmer, J.G. and Lovell, M.A. (1986) Natural enrichment of arsenic in Loch Lomond sediments. *Geochim. Cosmochim. Acta*, **50,** 2059-2067.

Farmer, J.G. (1994) Environmental change and the chemical record in Loch Lomond sediments. *Hydrobiologia*, **290,** 39-49.

Francus, P., von Suchodoletz, H., Dietze, M., Donner, R.V., Bouchard, F., Roy, A.-J., Fagot, M., Verschuren, D. and Kröpelin, S. (2013) Varved sediments of Lake Yoa (Ounianga Kebir, Chad) reveal progressive drying of the Sahara during the last 6100 years. *Sedimentology*, **60,** 911-934.

Gaiero, D.M., Probst, J.L., Depetris, P.J., Bidart, S.M. and Leleyter, L. (2003) Iron and other transition metals in Patagonian riverborne and windborne materials: geochemical control and transport to the southern South Atlantic Ocean. *Geochim. Cosmochim. Acta*, **67,** 3603-3623.

Gälman, V., Rydberg, J., Shchukarev, A., Sjöberg, S., Martínez-Cortizas, A., Bindler, R. and Renberg, I. (2009) The role of iron and sulfur in the visual appearance of lake sediment varves. *J. Paleolimnol.*, **42,** 141-153.

Garreaud, R.D., Vuille, M., Compagnucci, R. and Marengo, J. (2009) Present-day South American climate. *Palaeogeog. Palaeoclimatol. Palaeoecol.*, **281,** 180-195.

Gong, D. and Wang, S. (1999) Definition of Antarctic Oscillation index. *Geophys. Res. Lett.*, **26,** 459-462.

Granina, L., Karabanov, E. and Callender, E. (1993) Relics of oxidized ferromanganese formations in the bottom sediments of Lake Baikal. *IPPCCE Newsletter*, **7,** 32-39.

Granina, L., Müller, B. and Wehrli, B. (2004) Origin and dynamics of Fe and Mn sedimentary layers in Lake Baikal. *Chem. Geol.*, **205,** 55-72.

Granina, L.Z., Mats, V.D. and Phedorin, M.A. (2010) Iron-manganese formations in the Baikal region. *Russ. Geol. Geophys.*, **51,** 650-660.

Granina, L.Z., Zakharova, Y.P. and Parfenova, V.V. (2011) Biogenic Fe and Mn accumulation in the bottom sediments of Lake Baikal. *Geochem. Int.*, **49,** 1154.

Haberzettl, T., Corbella, H., Fey, M., Janssen, S., Lücke, A., Mayr, C., Ohlendorf, C., Schäbitz, F., Schleser, G.H., Wille, M., Wulf, S. and Zolitschka, B. (2007) Lateglacial and Holocene wet—dry cycles in southern Patagonia: chronology, sedimentology and geochemistry of a lacustrine record from Laguna Potrok Aike, Argentina. *Holocene*, **17,** 297-310.

Holmer, M. and Storkholm, P. (2001) Sulphate reduction and sulphur cycling in lake sediments: a review. *Freshwater Biol.*, **46,** 431-451.

Huerta-Diaz, M.A. and Morse, J.W. (1992) Pyritization of trace metals in anoxic marine sediments. *Geochim. Cosmochim. Acta*, **56,** 2681-2702.

Kestin, T.S., Karoly, D.J., Yano, J.-I. and Rayner, N.A. (1998) Time–Frequency Variability of ENSO and Stochastic Simulations. *J. Clim.*, **11,** 2258-2272.

Labuhn, I., Hammarlund, D., Chapron, E., Czymzik, M., Dumoulin, J.-P., Nilsson, A., Régnier, E., Robygd, J. and von Grafenstein, U. (2018) Holocene Hydroclimate Variability in Central Scandinavia Inferred from Flood Layers in Contourite Drift Deposits in Lake Storsjön. *Quaternary*, **1,** 1-24.

Lamy, F., Hebbeln, D., Röhl, U. and Wefer, G. (2001) Holocene rainfall variability in southern Chile: a marine record of latitudinal shifts of the Southern Westerlies. *Earth Planet. Sci. Lett.*, **185,** 369-382.

Lau, M.P., Niederdorfer, R., Sepulveda-Jauregui, A. and Hupfer, M. (2018) Synthesizing redox biogeochemistry at aquatic interfaces. *Limnologica*, **68,** 59-70.

Löwemark, L., März, C., O'Regan, M. and Gyllencreutz, R. (2014) Arctic Ocean Mn-stratigraphy: genesis, synthesis and inter-basin correlation. *Quat. Sci. Rev.*, **92,** 97-111.

Manning, P., Prepas, E. and Serediak, M. (1999) Pyrite and vivianite intervals in the bottom sediments of eutrophic Baptiste Lake, Alberta, Canada. *Can. Mineral.*, **37,** 593-601.

März, C., Stratmann, A., Matthiessen, J., Meinhardt, A.K., Eckert, S., Schnetger, B., Vogt, C., Stein, R. and Brumsack, H.J. (2011) Manganese-rich brown layers in Arctic Ocean sediments: Composition, formation mechanisms, and diagenetic overprint. *Geochim. Cosmochim. Acta*, **75,** 7668-7687.

Moy, C.M., Dunbar, R.B., Guilderson, T.P., Waldmann, N., Mucciarone, D.A., Recasens, C., Ariztegui, D., Austin Jr, J.A. and Anselmetti, F.S. (2011) A geochemical and sedimentary record of high southern

latitude Holocene climate evolution from Lago Fagnano, Tierra del Fuego. *Earth Planet. Sci. Lett.*, **302,** 1-13.

Müller, B., Granina, L., Schaller, T., Ulrich, A. and Wehrli, B. (2002) P, As, Sb, Mo, and Other Elements in Sedimentary Fe/Mn Layers of Lake Baikal. *Environ. Sci. Technol.*, **36,** 411-420.

Naeher, S., Gilli, A., North, R.P., Hamann, Y. and Schubert, C.J. (2013) Tracing bottom water oxygenation with sedimentary Mn/Fe ratios in Lake Zurich, Switzerland. *Chem. Geol.*, **352,** 125-133.

Nakagawa, T., Brugiapaglia, E., Digerfeldt, G., Reille, M., Beaulieu, J.-L.D. and Yasuda, Y. (1998) Dense-media separation as a more efficient pollen extraction method for use with organic sediment/deposit samples: comparison with the conventional method. *Boreas*, **27,** 15-24.

Ndiaye, M. (2007) *A multipurpose software for stratigraphic signal analysis*. PhD thesis, University of Geneva/Switzerland, 128 pp.

Och, L.M., Müller, B., Voegelin, A., Ulrich, A., Göttlicher, J., Steiniger, R., Mangold, S., Vologina, E.G. and Sturm, M. (2012) New insights into the formation and burial of Fe/Mn accumulations in Lake Baikal sediments. *Chem. Geol.*, **330,** 244-259.

Olivero, E.B. and Martinioni, D.R. (2001) A review of the geology of the Argentinian Fuegian Andes. *J. S. Am. Earth. Sci.*, **14,** 175-188.

Passier, H.F., Middelburg, J.J., de Lange, G.J. and Böttcher, M.E. (1999) Modes of sapropel formation in the eastern Mediterranean: some constraints based on pyrite properties. *Mar. Geol.*, **153,** 199-219.

Peterson, M.L. and Carpenter, R. (1986) Arsenic distributions in porewaters and sediments of Puget Sound, Lake Washington, the Washington coast and Saanich Inlet, B.C. *Geochim. Cosmochim. Acta*, **50,** 353-369.

Pohl, B., Fauchereau, N., Reason, C.J.C. and Rouault, M. (2010) Relationships between the Antarctic Oscillation, the Madden–Julian Oscillation, and ENSO, and Consequences for Rainfall Analysis. *J. Clim.*, **23,** 238-254.

Regnéll, J. and Everitt, E. (1996) Preparative centrifugation — a new method for preparing pollen concentrates suitable for radiocarbon dating by AMS. *Veg. Hist. Archaeobot.*, **5,** 201-205.

Renberg, I. (1986) Photographic demonstration of the annual nature of a varve type common in N. Swedish lake sediments. *Hydrobiologia*, **140,** 93-95.

Richter, T.O., van der Gaast, S., Koster, B., Vaars, A., Gieles, R., de Stigter, H.C., De Haas, H. and van Weering, T.C.E. (2006) The Avaatech XRF Core Scanner: technical description and applications to NE Atlantic sediments. In: *New techniques in sediment core analysis* (Ed R.G. Rothwell), **267,** pp. 39-50. Geological Society Special Publications, London.

Rogers, J.C. and Loon, H.v. (1982) Spatial Variability of Sea Level Pressure and 500 mb Height Anomalies over the Southern Hemisphere. *Mon. Weather Rev.*, **110,** 1375-1392.

Rohling, E.J., Marino, G. and Grant, K.M. (2015) Mediterranean climate and oceanography, and the periodic development of anoxic events (sapropels). *Earth-Sci. Rev.*, **143,** 62-97.

Shchukarev, A., Gälman, V., Rydberg, J., Sjöberg, S. and Renberg, I. (2008) Speciation of iron and sulphur in seasonal layers of varved lake sediment: an XPS study. *Surf. Interface Anal.*, **40,** 354-357.

Silvestri, G.E. and Vera, C.S. (2003) Antarctic Oscillation signal on precipitation anomalies over southeastern South America. *Geophys. Res. Lett.*, **30,** CLM 3-1 - 3-4.

Sobek, S., Durisch-Kaiser, E., Zurbrügg, R., Wongfun, N., Wessels, M., Pasche, N. and Wehrli, B. (2009) Organic carbon burial efficiency in lake sediments controlled by oxygen exposure time and sediment source. *Limnol. Oceanogr.*, **54,** 2243-2254.

Stern, C. (2008) Holocene tephrochronology record of large explosive eruptions in the southernmost Patagonian Andes. *Bull. Volcanol.*, **70,** 435-454.

Stern, C.R., Moreno, P.I., Henríquez, W.I., Villa-Martínez, R., Sagredo, E., Aravena, J.C. and de Pol-Holz, R. (2016) Holocene tephrochronology around Cochrane (~47°S), southern Chile. *Andean Geol.*, **43,** 1-19.

Tassone, A., Lippai, H., Lodolo, E., Menichetti, M., Comba, A., Hormaechea, J.L. and Vilas, J.F. (2005) A geological and geophysical crustal section across the Magallanes–Fagnano fault in Tierra del Fuego. *J. S. Am. Earth. Sci.*, **19,** 99-109.

Thomson, J., Croudace, I.W. and Rothwell, R.G. (2006) A geochemical application of the ITRAX scanner to a sediment core containing eastern Mediterranean sapropel units. In: *New techniques in sediment core analysis* (Ed R.G. Rothwell), **267**, pp. 65-77. Geological Society Special Publications, London.

Torres, N.T., Och, L.M., Hauser, P.C., Furrer, G., Brandl, H., Vologina, E., Sturm, M., Burgmann, H. and Muller, B. (2014) Early diagenetic processes generate iron and manganese oxide layers in the sediments of Lake Baikal, Siberia. *Environ. Sci. Process Impacts*, **16,** 879-889.

Villalba, R., Cook, E.R., D'Arrigo, R.D., Jacoby, G.C., Jones, P.D., Salinger, M.J. and Palmer, J. (1997) Sea-level pressure variability around Antarctica since A.D. 1750 inferred from subantarctic tree-ring records. *Clim. Dyn.*, **13,** 375-390.

Vogel, H., Wagner, B., Zanchetta, G., Sulpizio, R. and Rosén, P. (2010) A paleoclimate record with tephrochronological age control for the last glacial-interglacial cycle from Lake Ohrid, Albania and Macedonia. *J. Paleolimnol.*, **44,** 295-310.

Waldmann, N. (2008) *Late Quaternary environmental changes in Lago Fagnano, Tierra del Fuego (54°S): reconstructing sedimentary processes, natural hazards and paleoclimate*, University of Geneva, Geneva, Switzerland, 188 pp.

Waldmann, N., Ariztegui, D., Anselmetti, F.S., Austin Jr, J.A., Dunbar, R., Moy, C.M. and Recasens, C. (2008) Seismic stratigraphy of Lago Fagnano sediments (Tierra del Fuego, Argentina) - A potential archive of paleoclimatic change and tectonic activity since the Late Glacial. *Geol. Acta*, **6**, 101-110.

Waldmann, N., Ariztegui, D., Anselmetti, F.S., Austin, J.A., Moy, C.M., Stern, C., Recasens, C. and Dunbar, R.B. (2010a) Holocene climatic fluctuations and positioning of the Southern Hemisphere westerlies in Tierra del Fuego (54° S), Patagonia. *J. Quat. Sci.*, **25,** 1063-1075.

Waldmann, N., Ariztegui, D., Anselmetti, F.S., Coronato, A. and Austin Jr, J.A. (2010b) Geophysical evidence of multiple glacier advances in Lago Fagnano (54°S), southernmost Patagonia. *Quat. Sci. Rev.*, **29,** 1188-1200.

Waldmann, N., Anselmetti, F.S., Ariztegui, D., Austin, J.J.A., Pirouz, M., Moy, C.M. and Dunbar, R. (2011) Holocene mass-wasting events in Lago Fagnano, Tierra del Fuego (54°S): implications for paleoseismicity of the Magallanes-Fagnano transform fault. *Basin Res.*, **23,** 171-190.

Waldmann, N., Borromei, A.M., Recasens, C., Olivera, D., Martínez, M.A., Maidana, N.I., Ariztegui, D., Austin, J.A., Anselmetti, F.S. and Moy, C.M. (2014) Integrated reconstruction of Holocene millennial-scale environmental changes in Tierra del Fuego, southernmost South America. *Palaeogeog. Palaeoclimatol. Palaeoecol.*, **399,** 294-309.

FIGURES
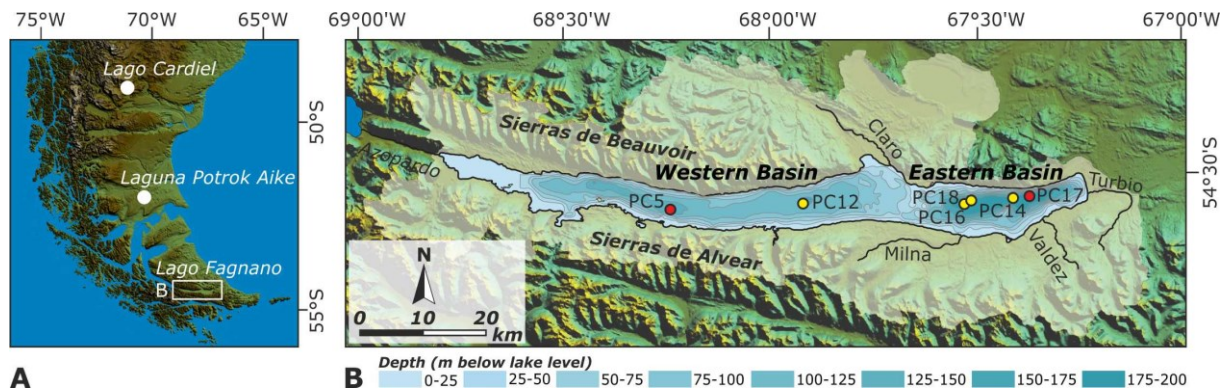
Figure 1. Regional setting of Lago Fagnano. **(A)** Location of Lago Fagnano (white box) on Tierra del Fuego and other lake records in southern South America; **(B)** Bathymetric map and watershed (white-shaded area) of Lago Fagnano including coring locations of cores analysed here (LF06-PC5 and -PC17; red dots) and from previous studies (Waldmann *et al.*, 2010a; Moy *et al.*, 2011; yellow dots).
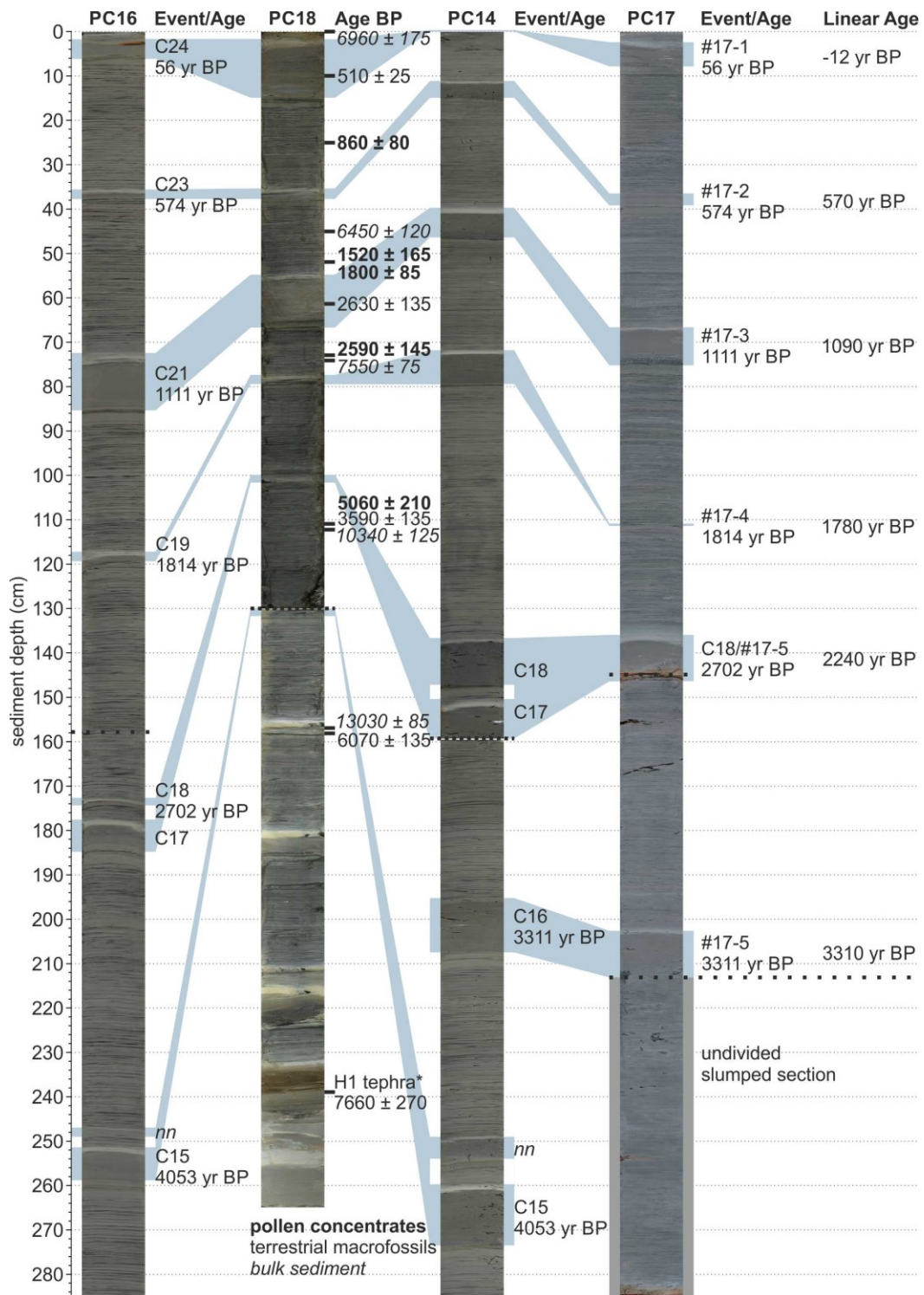
Figure 2. Event layer correlation between cores LF06-PC17 (this study), LF06-PC14 and LF06-PC16 (Waldmann *et al.*, 2011), and LF06-PC18 (Moy *et al.*, 2011). Ages in LF06-PC18 are radiocarbon dates (cal. yr BP ± 2σ), * mean pooled age of Stern (2008), as provided in Moy *et al.* (2011).
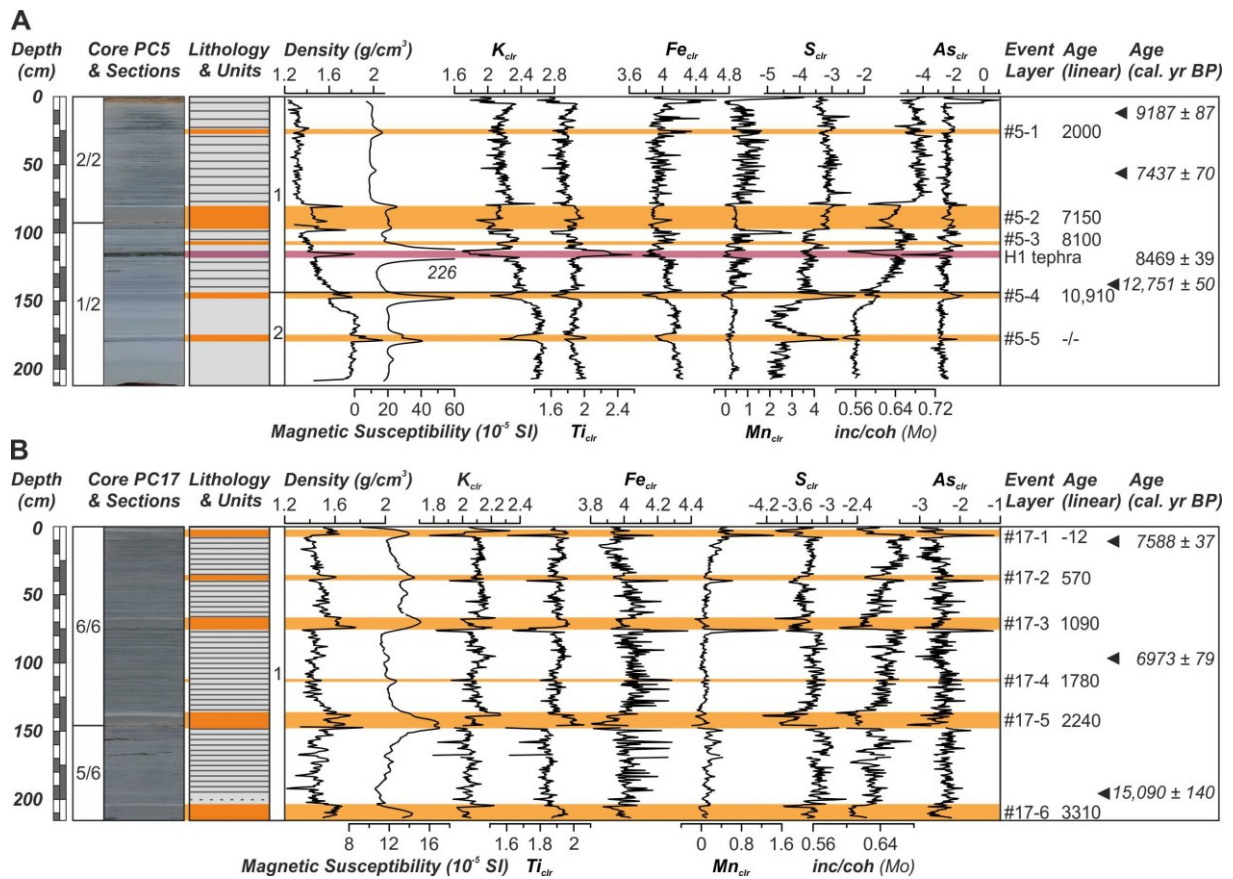
Figure 3. Lithology, density, magnetic susceptibility, µXRF, event layers and age estimates of cores **(A)** LF06-PC5, and **(B)** LF06-PC17 in the western and eastern sub-basins, respectively. XRF data are given as centred log-ratios (clr). Ages for event layers (orange bars) were calculated by linear interpolation based on the H1 Hudson tephra age (Stern *et al.*, 2016) for core LF06-PC5, and event stratigraphy for core LF06-PC17 following Waldmann *et al.* (2011) (applying a constant sedimentation rate of 0.52 mm/yr; see text and Fig. 2 for further explanation).
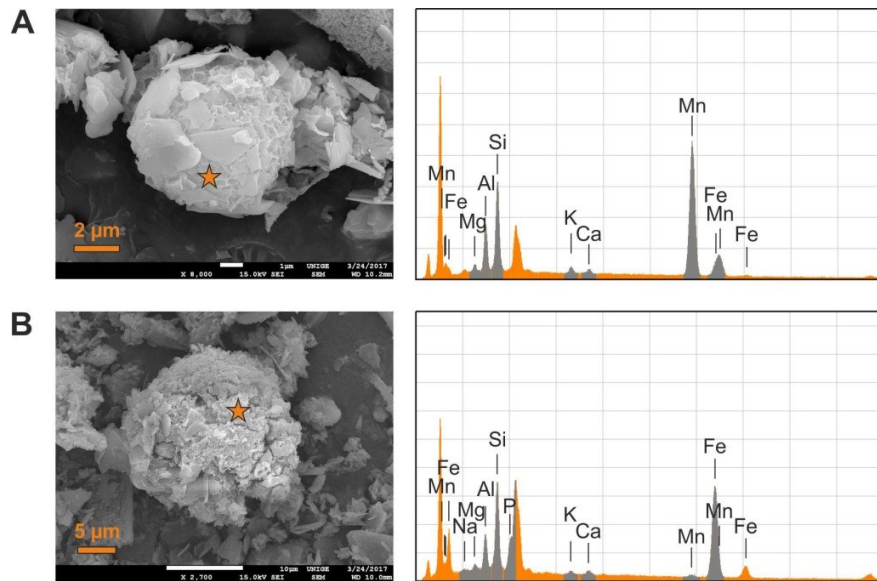
Figure 4. SEM photographs of **(A)** Mn-oxide (core LF06-PC5 at 1 cm sediment depth) and **(B)** Fe-oxide (core LF06-PC5 at 3 cm sediment depth) with corresponding EDS spectra. Orange stars denote the measurements positions. Note that clay minerals partly cover the oxides, producing minor peaks of e.g. Si, Al and K in the EDS spectra.
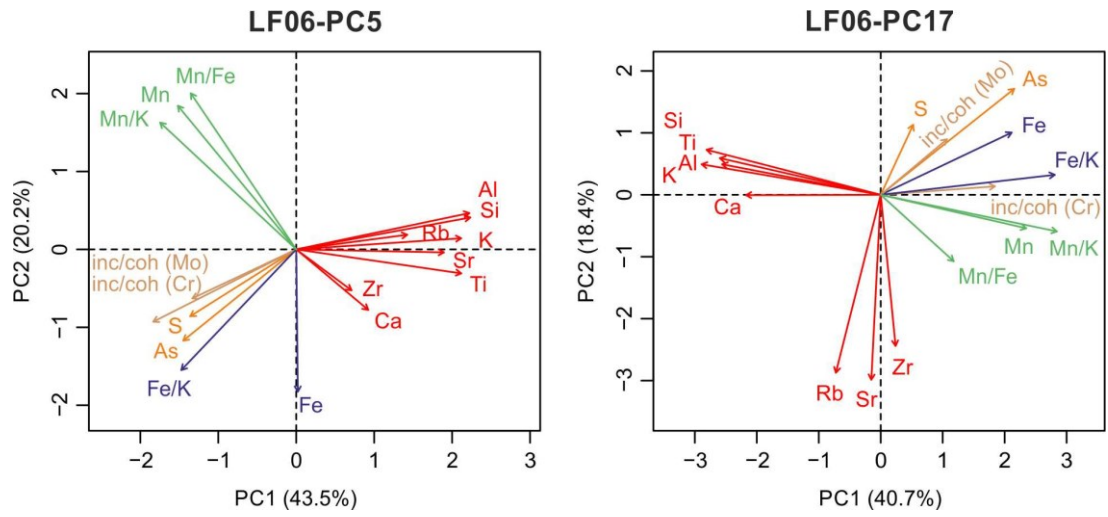
Figure 5. Principal component-biplots of XRF data for the laminated sections of cores LF06-PC5 and LF06-PC17. Mass-transported deposits were excluded from the datasets.
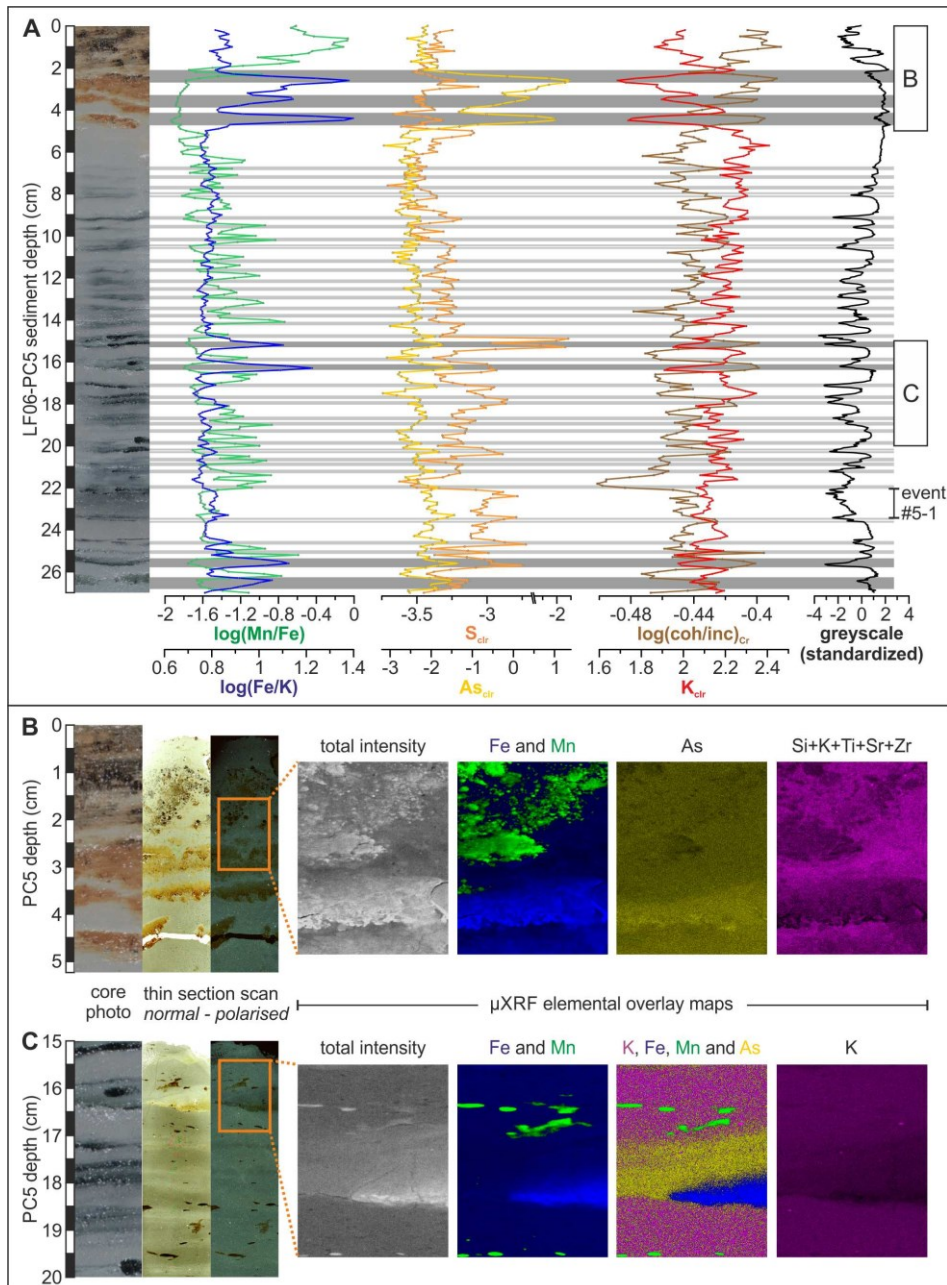
Figure 6. Characterisation of the lamination pattern in the western-central sub-basin of Lago Fagnano (core LF06-PC5). **(A)** XRF element scans of Mn/Fe, Fe/K, S, As, coh/inc and K for the topmost 27 cm (expressed as log-ratio or clr = centred log-ratio), and standardized greyscale of the core image that allowed defining laminae (grey horizontal bars, where dark-grey bars depict pronounced Fe peaks); **(B)** and **(C)**: core photos, thin section scans and μXRF elemental overlay maps of **(B)** the top-core brownish-black Mn- and orange-brown Fe-oxides, and **(C)** an exemplary greenish Fe-oxide lamina, followed by As enrichment and Mn patches.
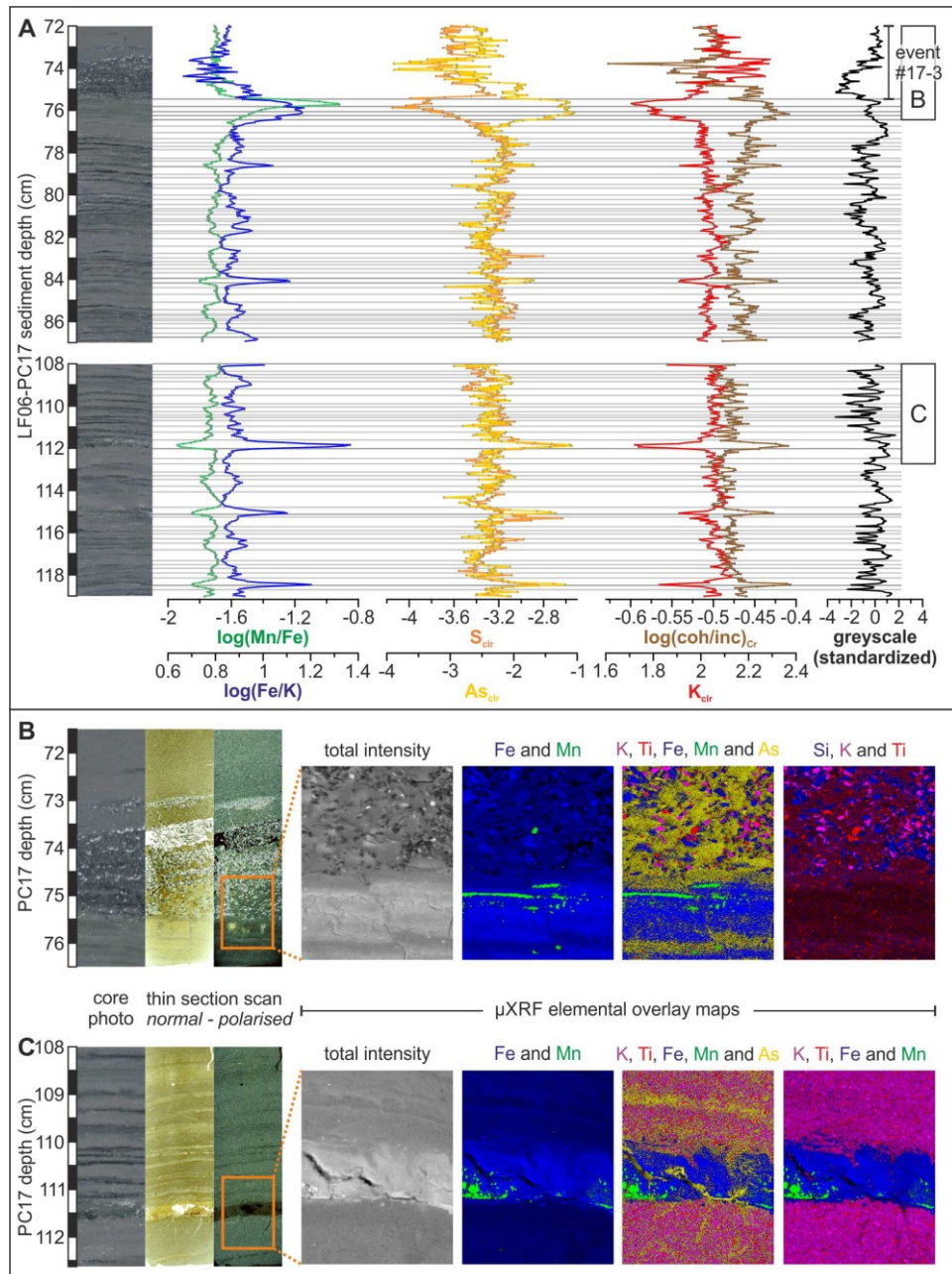
Figure 7. Characterisation of the lamination pattern in the eastern sub-basin of Lago Fagnano (core LF06-PC17). **(A)** As in Fig. 6, but for different depth intervals (72-87 cm and 108-119 cm); **(B)** and **(C)**: core photos, thin section scans and µXRF elemental overlay maps of **(B)** greenish, Fe- and Mn-enriched laminae followed by the coarse-grained base of a graded layer (event #17-3), and **(C)** an exemplary greenish Fe-oxide lamina (at 111.5 cm depth) that is enriched in As, S (not detectable by XRF mapping, but distinct S-peak in **(A)**) and some Mn, and a thin As-elevated lamina (at 111 cm depth).
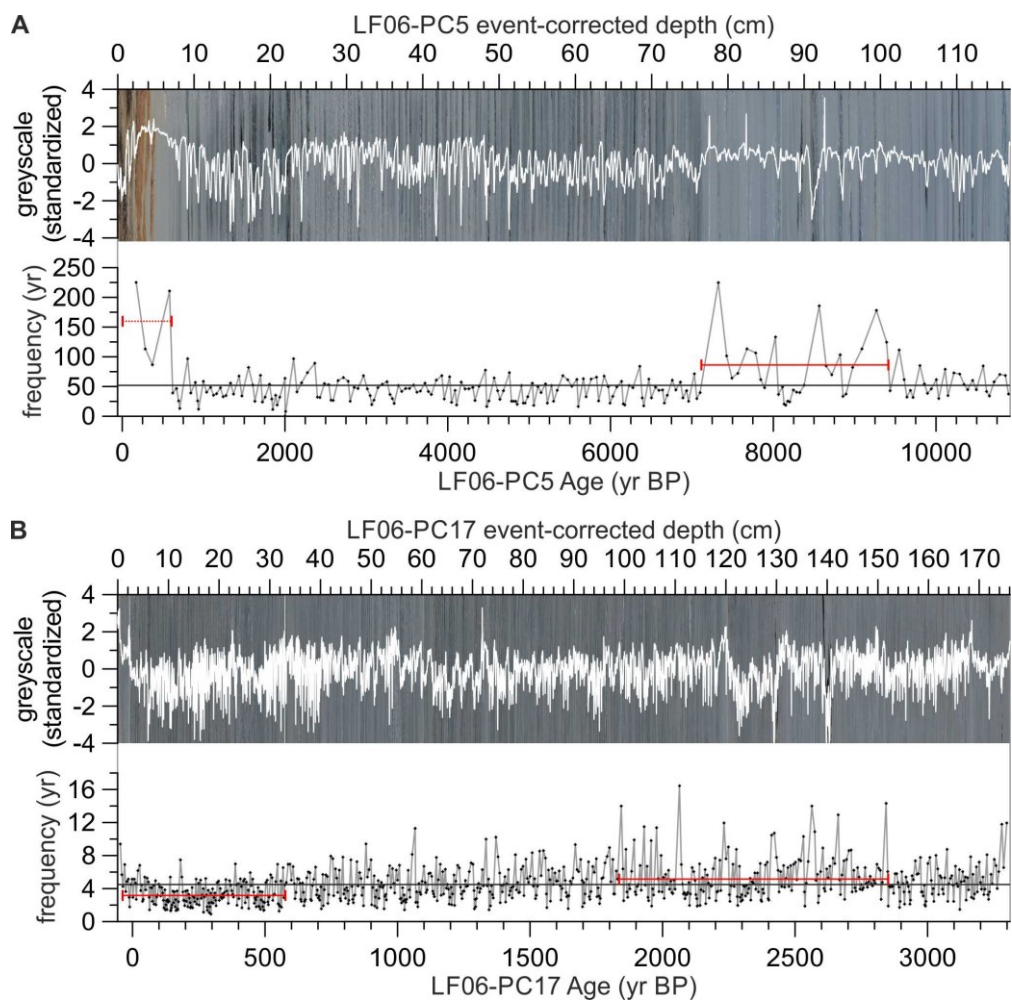
Figure 8. Standardized greyscale values and frequencies (in years) of black/greenish laminae in cores **(A)** LF06-PC5, and **(B)** LF06-PC17. Black (red) horizontal lines depict (distinct intervals of above/below-) average frequency values.
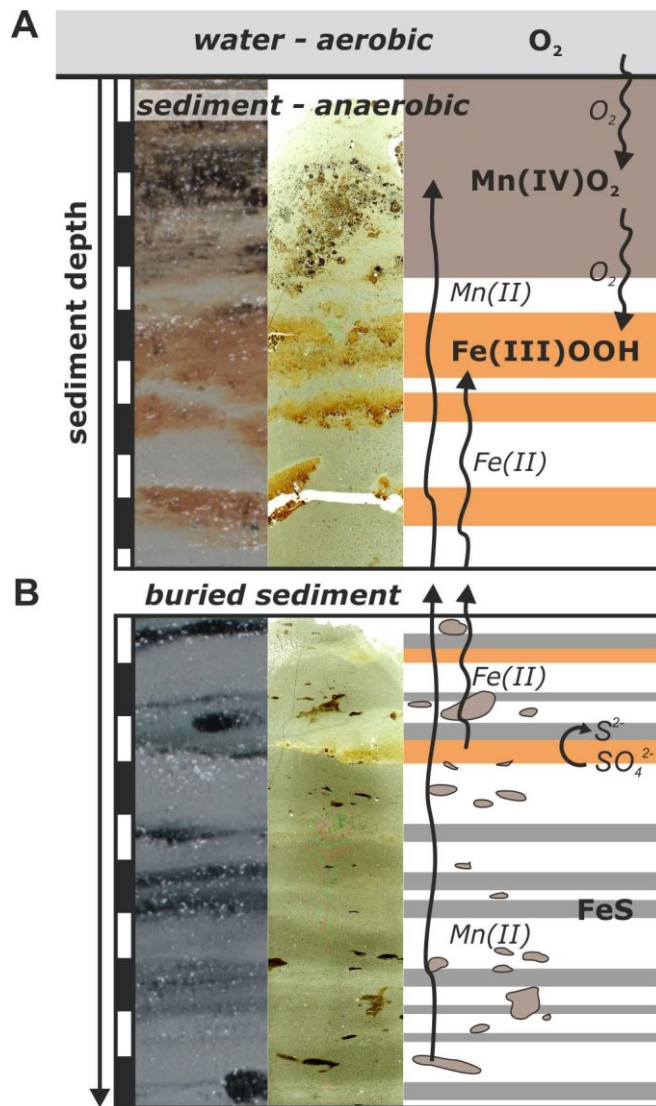
Figure 9. (A) Mechanism of formation of an active, dynamically growing redox front, and **(B)** early diagenetic dissolution and partial pyritisation of buried redox fronts in the sedimentary record of Lago Fagnano.

TABLES

Table 1. Radiocarbon dates of organic micro-remains extracted from cores LF06-PC5 and -PC17.

Lab-ID POZ-	Sample-ID (core_section_cm)	Core depth (m)	Event-free core depth (m)	Material	Age (^{14}C yr BP ± error)	Calibrated age (cal yr BP ± 1σ)
95359	PC5_2/2_10-14	0.12	0.12	40-50% charred particles 30-40% cf. phytoliths 10-20% pollen and spores 5-10% Pediastrum	8220 ± 50	9186 ± 87
95361	PC5_2/2_55-59.5	0.57	0.555	30-40% charred particles 30-40% algae/Pediastrum 20-30% pollen and spores 5-10% tissues 5-10% minerogen. particles	6520 ± 70	7434 ± 70
NN	PC5_1/2_21-24	1.16	0.91	Hudson (H1) tephra*	7683 ± 33	8469 ± 39
95360	PC5_1/2_41-50	1.38	1.125	50-60% pollen and spores 20-30% charred particles 10-20% minerogen. particles 10% algae	10,870 ± 60	12,751 ± 50
95357	PC17_6/6_8-14	0.11	0.07	60-70% tissues 30-40% charred particles 10% pollen and spores Few fungal remains	6720 ± 40	7588 ± 37
95358	PC17_6/6_95-99	0.97	0.815	50-60% tissues 30-40% charred particles 10% pollen and spores 10% fungal remains Few minerogen. particles	6100 ± 40	6973 ± 79
95355	PC17_5/6_47-52	1.96	1.68	40-50% tissues 30-40% pollen and spores 20% charred particles 5% algae	12,680 ± 70	15,090 ± 140

* Stern et al. (2016), mean age obtained from bulk sediment AMS ^{14}C dating from different lakes

Table 2. Correlation coefficients (R) of XRF element scanner data for laminated sections of cores LF06-PC5 (lower-left triangle) and LF06-PC17 (upper-right triangle). Event layers were excluded from the datasets; positive R values in bold.

	Al	Si	S	K	Ca	Ti	Mn	Fe	As	Rb	Sr	Zr	inc/coh Cr	inc/coh Mo	Mn/Fe	Fe/K	Mn/K
Al		**0.95**	-0.20	**0.61**	**0.32**	**0.43**	-0.59	-0.39	-0.45	**0.06**	-0.06	-0.29	-0.66	-0.39	-0.37	-0.56	-0.67
Si	**0.97**		-0.18	**0.73**	**0.47**	**0.60**	-0.63	-0.45	-0.47	-0.02	-0.14	-0.32	-0.63	-0.33	-0.37	-0.66	-0.74
S	-0.61	-0.52		-0.25	-0.41	-0.13	-0.30	**0.16**	**0.08**	-0.26	-0.21	-0.15	**0.11**	**0.08**	-0.38	**0.23**	-0.12
K	**0.88**	**0.87**	-0.46		**0.82**	**0.92**	-0.53	-0.56	-0.53	**0.02**	-0.20	-0.13	-0.32	-0.06	-0.22	-0.87	-0.77
Ca	**0.11**	**0.14**	-0.20	0.00		**0.83**	-0.20	-0.55	-0.46	0.00	-0.11	**0.00**	-0.09	**0.08**	**0.11**	-0.77	-0.45
Ti	**0.67**	**0.68**	-0.48	**0.62**	**0.67**		-0.50	-0.52	-0.51	-0.05	-0.24	-0.06	-0.16	**0.08**	-0.21	-0.80	-0.72
Mn	-0.43	-0.46	-0.01	-0.50	-0.41	-0.59		**0.25**	**0.42**	-0.18	-0.02	**0.02**	**0.41**	**0.29**	**0.85**	**0.43**	**0.95**
Fe	-0.01	-0.06	-0.03	**0.11**	**0.02**	**0.01**	-0.48		**0.47**	-0.30	-0.24	-0.09	**0.37**	**0.17**	-0.29	**0.89**	**0.40**
As	-0.55	-0.61	**0.17**	-0.56	-0.18	-0.52	-0.02	**0.45**		-0.63	-0.52	-0.46	**0.27**	**0.25**	**0.16**	**0.57**	**0.51**
Rb	**0.49**	**0.51**	-0.13	**0.75**	-0.21	**0.33**	-0.35	-0.06	-0.51		**0.88**	**0.65**	-0.20	-0.39	-0.02	-0.19	-0.14
Sr	**0.54**	**0.57**	-0.42	**0.44**	**0.60**	**0.75**	-0.47	-0.15	-0.54	**0.34**		**0.63**	-0.18	-0.43	**0.11**	-0.03	**0.06**
Zr	-0.01	**0.11**	**0.26**	**0.07**	**0.43**	**0.44**	-0.36	-0.25	-0.45	**0.26**	**0.54**		**0.34**	**0.16**	**0.06**	**0.02**	**0.06**
inc/coh Cr	-0.81	-0.75	**0.76**	-0.56	-0.21	-0.60	**0.17**	**0.15**	**0.40**	-0.19	-0.57	**0.13**		**0.71**	**0.20**	**0.39**	**0.43**
inc/coh Mo	-0.60	-0.49	**0.76**	-0.39	-0.11	-0.41	**0.10**	-0.11	**0.13**	-0.09	-0.44	**0.32**	**0.85**		**0.19**	**0.14**	**0.24**
Mn/Fe	-0.38	-0.40	0.00	-0.47	-0.37	-0.53	**0.98**	-0.63	-0.11	-0.29	-0.39	-0.26	**0.12**	**0.11**		-0.05	**0.72**
Fe/K	-0.62	-0.66	**0.30**	-0.62	**0.02**	-0.43	-0.03	**0.71**	**0.75**	-0.58	-0.43	-0.25	**0.51**	**0.19**	-0.17		**0.65**
Mn/K	-0.55	-0.57	**0.08**	-0.63	-0.37	-0.64	**0.99**	-0.45	**0.08**	-0.45	-0.50	-0.33	**0.25**	**0.16**	**0.97**	**0.09**	